Transients of the electromagnetically-induced-transparency-enhanced refractive Kerr nonlinearity: Theory

M. V. Pack,* R. M. Camacho, and J. C. Howell
Department of Physics, University of Rochester, Rochester, New York 14627, USA
(Received 2 March 2006; published 25 July 2006)

We present a theory describing the transients and rise times of the refractive Kerr nonlinearity which is enhanced using electromagnetically induced transparency (EIT). We restrict our analysis to the case of a pulsed signal field with continuous-wave EIT fields, and all fields are well below saturation. These restrictions enable the reduction of an EIT Kerr, four-level, density-matrix equation to a two-level Bloch-vector equation which has a simple and physically intuitive algebraic solution. The physically intuitive picture of a two-level Bloch vector provides insights that are easily generalized to more complex and experimentally realistic models. We consider generalization to the cases of Doppler broadening, many-level EIT systems (we consider the $D1$ line of ^{87}Rb), and optically thick media. For the case of optically thick media we find that the rise time of the refractive EIT Kerr effect is proportional to the optical thickness. The rise time of the refractive EIT Kerr effect sets important limitations for potential few-photon applications.

DOI: 10.1103/PhysRevA.74.013812 PACS number(s): 42.50.Gy, 42.65.Hw

I. INTRODUCTION

The large optical nonlinearities resulting from electromagnetically induced transparency (EIT) have created the potential for many low-light-level and few-photon applications [1–6]. The refractive Kerr, effect, in particular, has been the subject of much interest [7–11]. This optical nonlinearity results when a signal laser field ac-Stark-shifts one of the ground states in a Λ-type EIT system, perturbing the system away from Raman resonance and resulting in a cross phase shift between the signal and EIT laser fields (see Fig. 1). Schmidt and Imamoglu proposed the giant EIT Kerr nonlinearity and speculated that it may create "conditional phase shifts of the order of π with single photons, which should be beneficial for quantum nondemolition measurements of weak signals and quantum logic gate operation" [7]. For a review of EIT-enhanced nonlinear optics see Refs. [6,5].

For few-photon applications such as quantum nondemolition measurements and quantum-logic gates the signal field must be pulsed such that it contains only a small number of photons. Because the number of photons in a pulse is directly proportional to the product of the intensity and the quantization volume (the quantization volume being given by the pulse volume $V=Ac\tau_{pulse}$, where A is the pulse area, c is the speed of light, and τ_{pulse} is the pulse duration) and because the area A has a lower bound given by the diffraction limit, tailoring EIT optical nonlinearities to be responsive to few-photon pulses is essentially a trade-off between increasing low-light-level sensitivity and decreasing the rise time. Ultimately, few-photon applications require optical nonlinear processes that are both fast and low light level. Thus, quantum-optical and few-photon applications require a sound understanding of the optical nonlinearity's transients and the trade-offs between optical intensity and pulse duration.

Initial proposals for the absorptive [12] and refractive [7] EIT Kerr nonlinearities limited their treatments to the continuous-wave (cw) or quasi-cw regime. More recent treatments discuss some time-dependent aspects. Transients of the absorptive Kerr effect for a pulsed signal and cw EIT fields have been well studied both theoretically [13] and experimentally [14–16]. Several researchers have also considered the dynamics of pulsed EIT fields for both types of Kerr effects [4,8,17].

Recently, refractive EIT Kerr transients for the case of pulsed signal fields have also drawn increased attention. For example, Deng *et al.* used Fourier transforms of coupled amplitude and Maxwell equations to derive a complex double integral describing the refractive EIT Kerr dynamics in the short-signal-pulse limit [18]. This solution has the limitation that the signal pulse must be very short and weak such that ground-state coherence "can be frozen out during the calculation of the nonlinear response" [18]. Also, Ottaviani *et al.*

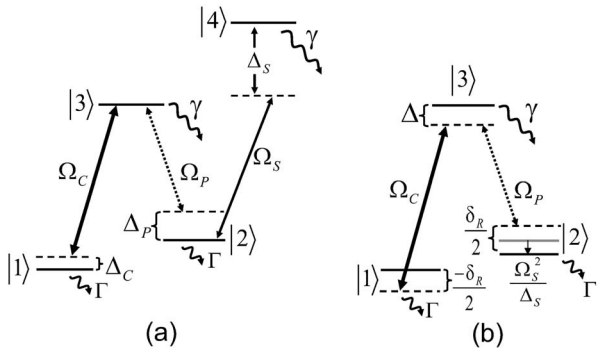

FIG. 1. Simple EIT Kerr system with four levels (a) and a three-level approximation to the EIT Kerr system (b). The detunings are defined as $\Delta_P \equiv (\omega_3-\omega_2)-\omega_P$, $\Delta_C \equiv (\omega_3-\omega_1)-\omega_C$, $\Delta_S \equiv (\omega_4-\omega_2)-\omega_S$, $\Delta \equiv (\Delta_P+\Delta_C)/2$, and $\delta_R \equiv \Delta_P-\Delta_C$. Also, the Rabi frequencies are defined as $\Omega_i \equiv \mu_i E_i/\hbar$ where $i=\{P,C,S\}$, μ_i is the dipole moment, and E_i is the electric field. The spontaneous emission rate out of the excited state is given by γ, and Γ is the decoherence rate for the ground states.

*Electronic address: mvpack@pas.rochester.edu

have shown theoretically that, in a five-level M system, a fast two-qubit quantum phase gate can be realized due to the transients arising from a pulsed signal [19].

EIT Kerr dynamics are also closely related to the more general topic of coherent transients in multilevel systems. Chen *et al.* and Park *et al.* have observed absorption transients in Λ-EIT media induced by rapid changes to the Raman—i.e., two-photon—detuning [20,21]. Similarly, Godone *et al.* have observed transients due to phase modulation of Raman beams in a Λ system [22]. Many others have also studied transients in three-level EIT systems under a number of different contexts such as coherent Raman beats [23], lasing without inversion [24–26], Zeeman splitting [27–29], adiabatic rapid passage [30,31], EIT in semiconductors [32,33], and coherent population trapping in closed-loop systems [34,35].

In this paper we use a density matrix formalism to derive simple analytic expressions for the evolution of a perturbed Λ-EIT system in the weak-field limit (the weak-field limit assumes that all Rabi frequencies are much smaller than the spontaneous emission rates). Using a reduction of the density matrix to a two-level Bloch equation [36], we show that the susceptibilities are primarily determined by the evolution of the ground-state coherences. From these transient solutions we derive the nonlinear susceptibilities and their rise times. Finally, we show how insights obtained from studying the optically thin Λ system apply to more physically realistic models of EIT systems in which Doppler broadening, optically thick media, and more than three EIT levels are included.

II. TRANSIENTS DUE TO PERTURBATIONS IN A Λ SYSTEM

Figures 1(a) and 1(b) show the reduction of a four-level N system to three-level Λ system with the Stark shift due to Ω_S explicitly accounted for. This is one of the simplest systems displaying EIT Kerr optical nonlinearities.

Levels $|1\rangle$, $|3\rangle$, and $|2\rangle$ together with the probe and coupling fields Ω_P and Ω_C make the Λ-EIT system. The Rabi frequencies, detunings, and decay rates are defined in the caption of Fig. 1. The far-detuned signal field Ω_S ac-Stark-shifts state $|2\rangle$ and modifies the probe detuning such that $\Delta_P(\Omega_S)=\Delta_P(0)+\Omega_S^2/\Delta_S$. In Fig. 1(b) we explicitly account for the Stark shift by shifting the energy of level $|2\rangle$ by $-\Omega_S^2/\Delta_S$ and removing the signal beam. In Fig. 1(b), we also introduce the one-photon detuning $\Delta\equiv(\Delta_P+\Delta_C)/2$ and two-photon detuning (Raman detuning) $\delta_R\equiv\Delta_P-\Delta_C$. The definitions for all detunings are such that the detunings are all positive as depicted in Figs. 1(a) and 1(b).

In addition to shifting the energy of level $|2\rangle$, the signal field also increases the decoherence rate for level $|2\rangle$ by $\Omega_S^2\gamma/\Delta_S^2$. However, by choosing the signal detuning sufficiently large the increased decoherence can be negligible while the Stark shift remains significant. Thus, we assume large signal detuning and ignore the increased decoherence.

The model for the refractive EIT Kerr effect is simply a three-level system in which the two-photon detuning undergoes a sudden perturbation. Therefore, we expect the transients to be similar to other perturbations that create sudden changes in Raman detuning such as frequency modulating the laser frequency [20,21] or Zeeman splitting [27,28].

Before specializing to the case of Stark shifts, we derive analytic expressions for transients due to general perturbations to the Λ system. In the next section we return to the special case of Stark shifts. The Hamiltonian describing the coherent evolution of Fig. 1(b) is given by

$$\hat{H}=\hbar\begin{pmatrix}\frac{\delta_R}{2} & 0 & \frac{\Omega_C^*}{2}\\ 0 & -\frac{\delta_R}{2} & \frac{\Omega_P^*}{2}\\ \frac{\Omega_C}{2} & \frac{\Omega_P}{2} & \Delta\end{pmatrix}. \tag{1}$$

Including the decay and decoherence terms shown in Fig. 1(b) and going to a rotating reference frame, the density matrix equations describing the evolution of the atoms are

$$\dot{\rho}_{33}=-\gamma\rho_{33}+\mathrm{Im}(\Omega_2^*\rho_{32}+\Omega_1^*\rho_{31}), \tag{2}$$

$$\dot{\rho}_{22}=\frac{\gamma}{2}\rho_{33}-\Gamma\left(\rho_{22}-\frac{1}{2}\right)-\mathrm{Im}(\Omega_2^*\rho_{32}), \tag{3}$$

$$\dot{\rho}_{11}=\frac{\gamma}{2}\rho_{33}-\Gamma\left(\rho_{11}-\frac{1}{2}\right)-\mathrm{Im}(\Omega_1^*\rho_{31}), \tag{4}$$

$$\dot{\rho}_{32}=[i(\Delta-\delta_R/2)-\Gamma_\perp]\rho_{32}+i\frac{\Omega_P}{2}(\rho_{22}-\rho_{33})+i\frac{\Omega_1}{2}\rho_{21}^*, \tag{5}$$

$$\dot{\rho}_{31}=[i(\Delta+\delta_R/2)-\Gamma_\perp]\rho_{31}+i\frac{\Omega_C}{2}(\rho_{11}-\rho_{33})+i\frac{\Omega_2}{2}\rho_{21}, \tag{6}$$

$$\dot{\rho}_{21}=(i\delta_R-\Gamma)\rho_{21}-i\frac{\Omega_C}{2}\rho_{32}^*+i\frac{\Omega_P^*}{2}\rho_{31}, \tag{7}$$

where $\Gamma_\perp=(\gamma+\Gamma)/2$ is the transverse decay rate for coherences with the excited state. The spontaneous emission from the excited state, at rate γ, repopulates both ground states with equal probability. The ground-state decay rate Γ is due to diffusion of coherent atoms out of the laser beam and diffusion of maximally mixed thermal atoms into the beam (the energy between ground states, $\hbar|\omega_1-\omega_2|$, is assumed to be much less than the thermal energy k_BT).

When the two-photon detuning is zero, the dark state

$$|-\rangle\equiv\frac{\Omega_P|1\rangle-\Omega_C|2\rangle}{\sqrt{\Omega_P^2+\Omega_C^2}} \tag{8}$$

becomes an energy eigenstate of the Hamiltonian and is decoupled from the excited state. Additionally, the bright state, which is the superposition of ground states orthogonal to the dark state, is coupled to the excited state with Rabi frequency $\Omega=\sqrt{\Omega_P^2+\Omega_C^2}$. As atoms are excited from the bright state and

spontaneously decay, there is a 50% probability they will decay into the dark state and become trapped. This is known as coherent population trapping (CPT) and is a common mechanism for obtaining EIT.

When the two-photon detuning is nonzero, the dark state is still a useful concept, even though it is no longer an energy eigenstate. The dark state is always the coherent superposition of ground states for which all probability amplitudes for excitation destructively interfere completely. Because the dark state describes the interference between excitation amplitudes and this interference is crucial to understanding the optical susceptibilities, the density matrix elements for the dark state—i.e., $\rho_{11}^{(-)}=|\Omega_P|^2/\Omega^2$, $\rho_{22}^{(-)}=|\Omega_C|^2/\Omega^2$, and $\rho_{21}^{(-)}=-\Omega_C\Omega_P^*/\Omega^2=-e^{i\theta}|\Omega_C\Omega_P|/\Omega^2$ where $(-)$ denotes the dark state—reoccur often in equations throughout this paper.

In order to obtain simple analytical solutions to Eqs. (2)–(7) we restrict our analysis to the weak-field–low-light limit (i.e., $\Omega \ll \gamma$). We also assume the EIT condition $\Omega^2 \gg \gamma\Gamma$ is satisfied. The low-light assumption justifies adiabatically eliminating the excited-state coherences, and as shown by Bennink in Ref. [36] the excited-state coherences become

$$\rho_{32} \approx -\frac{\frac{\Omega_P}{2}(\rho_{22}-\rho_{33})+\frac{\Omega_C}{2}\rho_{21}^*}{\Delta+i\Gamma_\perp} \tag{9}$$

and

$$\rho_{31} \approx -\frac{\frac{\Omega_C}{2}(\rho_{11}-\rho_{33})+\frac{\Omega_P}{2}\rho_{21}}{\Delta+i\Gamma_\perp}. \tag{10}$$

Bennink [36] also shows that the remaining master equations (2)–(4) and (7) reduce to a two-level Bloch vector equation for the ground states,

$$\frac{d}{dt}\vec{\rho}=(R+\Gamma)[-\vec{\rho}+\vec{T}\times\vec{\rho}+(1-3\rho_{33})\vec{F}], \tag{11}$$

and a first-order differential equation

$$\frac{d}{dt}\rho_{33}=-\gamma\rho_{33}-(R+\Gamma)\vec{\rho}\cdot\vec{F}+(1-3\rho_{33})R. \tag{12}$$

In the above we have used the following definitions:

$$\vec{\rho}\equiv\begin{pmatrix}u\\v\\w\end{pmatrix}=\begin{pmatrix}2\,\mathrm{Re}(e^{-i\theta}\rho_{21})\\2\,\mathrm{Im}(e^{-i\theta}\rho_{21})\\\rho_{22}-\rho_{11}\end{pmatrix}, \tag{13}$$

$$\vec{F}\equiv\frac{R(1-3\rho_{33})}{R+\Gamma}\begin{pmatrix}2e^{-i\theta}\rho_{21}^{(-)}\\0\\\rho_{22}^{(-)}-\rho_{11}^{(-)}\end{pmatrix}, \tag{14}$$

$$\vec{T}\equiv\frac{\delta_R}{R+\Gamma}\hat{w}+\frac{\Delta}{\Gamma(1-3\rho_{33})}\vec{F}, \tag{15}$$

$$R\equiv\frac{\Omega^2\Gamma_\perp/4}{\Delta^2+\Gamma_\perp^2}, \tag{16}$$

where $\hat{w}=(0,0,1)^T$ is the unit vector in the direction of w and without loss of generality we will assume $\theta=0$. The use of the symbols $\vec{T}$ and $\vec{F}$ is intentionally suggestive of a torque and a force, and although $\vec{T}$ and $\vec{F}$ are dimensionless and not forces, we will refer to them as the torque and force vector. To avoid confusion we note that there are no true forces discussed in this paper.

It has also been shown in Ref. [36] that the steady-state solutions to Eqs. (11) and (12) are

$$\vec{\rho}^{ss}=(1-3\rho_{33})\frac{\vec{F}+\vec{T}\times\vec{F}+\vec{T}(\vec{T}\cdot\vec{F})}{1+T^2} \tag{17}$$

and

$$\rho_{33}^{ss}=\frac{R-(R+\Gamma)\vec{F}\cdot\vec{\rho}\big|_{\rho_{33}=0}}{\gamma+3[R-(R+\Gamma)\vec{F}\cdot\vec{\rho}\big|_{\rho_{33}=0}]}, \tag{18}$$

where $T=|\vec{T}|$.

The weak-field approximation implies that $\rho_{33}\ll 1$ and the term ρ_{33} can be ignored and dropped in Eqs. (11) and (17). Thus, the three-level density-matrix problem reduces to a two-level Bloch-vector equation.

Setting $\rho_{33}=0$, we solve Eq. (11) for a constant perturbation at time $t\geqslant 0$. By rotating into a new primed coordinate system such that $\vec{T}'$ lies along the new w' axis, Eq. (11) decouples into three separate ordinary differential equations

$$\left(\frac{d^2}{d\tau^2}+2\frac{d}{d\tau}+1+T^2\right)\begin{Bmatrix}u'-u_f'\\v'-v_f'\end{Bmatrix}=0 \tag{19}$$

and

$$\left(\frac{d}{d\tau}+1\right)(w'-w_f')=0, \tag{20}$$

where $\tau=(R+\Gamma)t$. The initial conditions are given by $\vec{\rho}(0)=\vec{\rho}_i$ and

$$\dot{u}'(0)=-Tv_i'-u_i'+(1+T^2)u_f' \tag{21}$$

and

$$\dot{v}'(0)=Tu_i'-v_i'. \tag{22}$$

The subscript f denotes the final steady-state values which are derived from Eq. (17) with $\rho_{33}=0$.

The solutions are

$$u'(\tau)-u_f'=Ae^{-\tau}\cos(T\tau+\phi) \tag{23}$$

and

$$v'(\tau)-v_f'=Ae^{-\tau}\sin(T\tau+\phi), \tag{24}$$

$$w'(\tau)-w_f'=(w_i'-w_f')e^{-\tau}, \tag{25}$$

where

$$\tan\phi = \frac{v_f' - v_i'}{u_f' - u_i'} \tag{26}$$

and

$$A = \frac{u_i' - u_f'}{\cos\phi} = \frac{v_i' - v_f'}{\sin\phi}. \tag{27}$$

The conversion back to the unprimed coordinate system is

$$\begin{pmatrix} u \\ v \\ w \end{pmatrix} = \frac{1}{T}\begin{pmatrix} T_w & 0 & T_u \\ 0 & T & 0 \\ -T_u & 0 & T_w \end{pmatrix}\begin{pmatrix} u' \\ v' \\ w' \end{pmatrix}. \tag{28}$$

It is straightforward to apply this solution to more complicated piecewise constant perturbations by solving each piecewise constant segment separately using the above formalism.

Finally, since we are primarily interested in atom-photon interactions, we derive the probe and coupling susceptibilities which are

$$\chi_P = \frac{N|\mu_{32}|^2}{\epsilon_0 \hbar \Omega_P}\rho_{32} \tag{29}$$

and

$$\chi_C = \frac{N|\mu_{31}|^2}{\epsilon_0 \hbar \Omega_C}\rho_{31}, \tag{30}$$

where N is the number of atoms, μ is the dipole moment, and the remaining terms have their usual meanings. The susceptibilities simplify significantly if we assume moderate to small two-photon detuning ($\gamma \gg \delta_R$). This moderate-two-photon-detuning assumption is not very restrictive since most EIT measurements are performed with a two-photon detuning near the same order of magnitude as the optical pumping rate R and we have already assumed the fields and pumping to be weak. Also, the moderate-two-photon-detuning assumption justifies the approximations $\rho_{11} \approx |\Omega_P|^2/\Omega^2$ and $\rho_{22} \approx |\Omega_C|^2/\Omega^2$, and Eqs. (9) and (10) can be rewritten as

$$\rho_{32} \approx \frac{\rho_{22}\Omega_P(1 - \rho_{21}/\rho_{21}^{(-)})^*}{2(\Delta + i\Gamma_\perp)} \tag{31}$$

and

$$\rho_{31} \approx \frac{\rho_{11}\Omega_C(1 - \rho_{21}/\rho_{21}^{(-)})^*}{2(\Delta + i\Gamma_\perp)}. \tag{32}$$

The only term in Eqs. (31) and (32) significantly affected by perturbations to the two-photon detuning is the ground-state coherence ρ_{21}. Thus, we see that to a good approximation the changes in the probe and coupling susceptibilities are predominantly determined by the ground-state coherence.

III. DYNAMICS OF EIT KERR REFRACTIVE SWITCHING

The susceptibilities consist of a linear part $\chi_p^{(1)}$ which is field independent and a nonlinear term which is field dependent (i.e., $\chi_P = \chi_P^{(1)} + \chi_P^{(3)}|E_S|^2 + \chi_P^{(5)}|E_S|^4 + \cdots$). The cross Kerr effect is given by $\chi_P^{(3)}$, which in steady state can be found by taking the limit

$$\chi_P^{(3)} = \lim_{E_S \to 0} \frac{\chi_P(E_S) - \chi_P(0)}{|E_S|^2}.$$

Because we will see that the dynamics depends on the size of the signal field, we do not restrict ourselves to this limit. Instead, we define the dynamical Kerr nonlinearity as

$$\begin{aligned} \mathcal{X}_{Kerr}(\Omega_S, t) &\equiv \sum_{n=0}^{\infty} \chi_P^{(2n+3)}|E_S|^{2n} \\ &= \frac{|\mu_{32}|^4[\chi_P(t) - \chi_P(0)]}{\hbar^2|\Omega_S|^2} \\ &= -i\frac{N|\mu_{32}|^4}{\epsilon_0\hbar}\frac{\Delta u - i\Delta v}{2\hbar^2|\Omega_S|^2(\Delta + i\Gamma_\perp)}, \end{aligned} \tag{33}$$

where $\Delta u = u(\tau) - u_i$ and $\Delta v = v(\tau) - v_i$; at time $t=0$ the atoms are in steady state with $\Omega_S = 0$ and for time $t > 0$ Ω_S is a constant. Although referring to $\mathcal{X}_{Kerr}$ as the Kerr nonlinearity is a bit of a misnomer, it preserves the idea of a field-dependent change in the index of refraction, and in the limit of small signal field $\mathcal{X}_{Kerr}$ approaches the true definition of Kerr nonlinearity. Finally, the only time-dependent terms in Eq. (33) are the real and imaginary parts u and v of the ground-state coherence. Thus, it is sufficient to look at the evolution of u and v in order to understand the transients of the EIT Kerr nonlinearity.

For the refractive EIT Kerr effect we are primarily interested in the case in which the unperturbed system is in Raman resonance; i.e., the two-photon detuning is zero. Figure 2 shows the evolution of u and v for the somewhat artificial case when $\Delta(\Omega_S) = \Delta(0) = 0$, $\Omega_C = 10^{-2}\gamma$, $\Omega_P = 10^{-3}\gamma$,

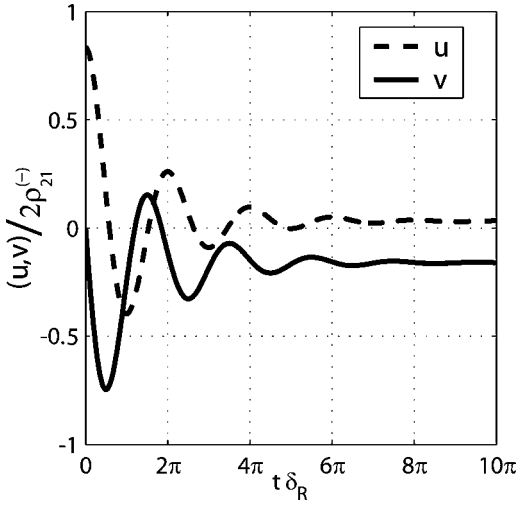

FIG. 2. Time dynamics of u and v for the special case of a single velocity class with $\Delta = 0$, $\Omega_C = 10^{-2}\gamma$, $\Omega_P = 10^{-3}\gamma$, and $\Gamma = 10^{-5}\gamma$. Initially the atom is prepared with $\delta_R = 0$. Thus, the atoms are as close to the dark state as the nonzero decoherence rate Γ allows. At time $t=0$ there is a sudden change such that $\delta_R = -3\Omega^2/\gamma \approx -3/2R$ and all other parameters remain the same.

$\Gamma=10^{-5}\gamma\delta_R(0)=0$, and $\delta_R(\Omega_S)=3\Omega^2/\gamma\approx 3R$. This choice of parameters was motivated by the fact that for $\Delta=0$ the dynamics and steady state are constrained to the same plane; i.e., the prime and unprimed coordinate systems are the same, making them easier to plot. Chen *et al.* and Park *et al.* have observed absorption transients which are very similar to u in Fig. 2 [20,21].

There are several features of the atomic evolution which merit discussion. First, the atoms evolve toward their new steady state via damped harmonic oscillations with decay constant $R+\Gamma$ and oscillation frequency $T(R+\Gamma)$. These two time constants suggest dividing the dynamics into two regimes: a large-torque regime and a small-torque regime. In the large-torque regime in which $T>1$ $(\delta_R>R)$ the oscillations dominate the exponential decay. This is the regime shown in Fig. 2. In the small-torque regime in which $T<1$ $(\delta_R<R)$ the exponential decay dominates. In the small-torque regime $\mathcal{X}_{Kerr}$ approaches the true definition of the Kerr nonlinearity.

The u and v rise times change significantly depending on whether they are in the small- or large-torque regime. Figure 3 shows a log-log plot of the $1/e$ rise times for u and v versus induced two-photon detuning. The same parameters as those in Fig. 2 are used. For small two-photon detunings—i.e., in the small-torque regime—the rise times asymptotically approach constants

$$\lim_{\delta_R\to 0} t_u = \frac{1+\ln\{2+\ln[2+\ln(2+\cdots)]\}}{R+\Gamma} \tag{34}$$

and

$$\lim_{\delta_R\to 0} t_v = \frac{1}{R+\Gamma}. \tag{35}$$

These rise times can be understood by considering that the phase of the ground-state coherence—i.e., $\theta=\arg(\rho_{21}/\rho_{21}^{(-)})$—increases at approximately the two-photon detuning rate $(\dot{\theta}\approx\delta_R)$. Also, u and v approach their final values when the change in θ approaches $\Delta\theta\approx\delta_R/(R+\Gamma)$. Thus, the rise times are approximately the ratio of the rotation rate and rotation angle of θ $[t\approx\Delta\theta/\dot{\theta}=(R+\Gamma)^{-1}]$. Since both the rotation rate and rotation angle have the same dependence on δ_R for $T<1$, the rise times are constants.

For large detunings—i.e., the large-torque regime—the rise times asymptotically approach the curves

$$\lim_{\delta_R\to\infty} t_u = \frac{\arccos[e^{-1}+(R+\Gamma)/\delta_R]}{\delta_R} \tag{36}$$

and

$$\lim_{\delta_R\to\infty} t_v = \frac{(1-e^{-1})(R+\Gamma)}{\delta_R^2}. \tag{37}$$

To understand these rise times physically we once again consider the ratio between the rotation rate $\dot{\theta}\approx\delta_R$ and rotation angle $\Delta\theta$. The coherence first approaches its final value of v for a phase angle of $\Delta\theta\approx(R+\Gamma)/\delta_R$, giving $t_v\approx(R+\Gamma)/\delta_R^2$. u approaches its final value for $\Delta\theta\approx\pi/2$, resulting in $t_u\approx\pi/2\delta_R$. For very large Stark shifts the moderate-two-photon-detuning approximation breaks down.

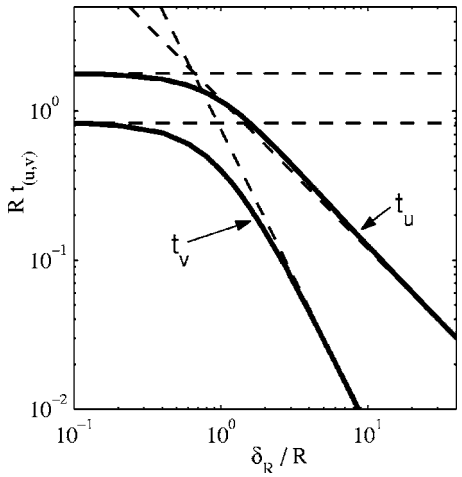

FIG. 3. Solid lines show the $1/e$ rise time for the real part u (imaginary part v) of the ground-state coherence plotted logographically as a function of the magnitude of the two-photon detuning δ_R. All quantities are dimensionless and normalized by the optical pumping rate R, and $\Gamma/R=0.2$. For small detunings the rise times asymptotically approach $t_u\approx 2.15/(R+\Gamma)$ and $t_v=1/(R+\Gamma)$. For large two-photon detunings the rise times asymptotically approach $t_u\approx 1.2/\delta_R$ and $t_v\approx 0.63(R+\Gamma)/\delta_R^2$. The asymptotes are shown as dashed lines.

In the large-torque regime the coherence and susceptibilities can significantly overshoot their final steady-state values. As u goes from positive to negative the susceptibility goes from EIT to EIA (electromagnetically induced absorption). For EIA the interference paths for absorption constructively interfere and the absorption is greater than it would be for the case of completely incoherent probe and coupling fields. EIA has been observed for transients due to rapid changes of Raman detuning [20,21].

Plotting v versus u parametrically as a function of time yields the spiral plot (dashed line) shown in Fig. 4. This plot suggests the analogy between $\vec{T}$ and a torque. The steady-state values, shown as the solid line in Fig. 4, are those values for which the "torque" $\vec{T}\times\vec{\rho}$, and the analogs to "force" vectors—i.e., the optical pumping "force" $\vec{F}$ and decay $-\vec{\rho}$—balance each other. When a new "torque" is introduced the phase θ increases until damping mechanisms—i.e., optical pumping and decoherence—bring it to its new steady-state value. The unit circle in Fig. 4 shows the largest possible values for u and v.

IV. GENERALIZATIONS TO REALISTIC MODELS

The intuitive picture of coherences spiraling to their new steady-state values is helpful in generalizing the three-level EIT Kerr calculations to more realistic models which include Doppler broadening, additional atomic levels, and optically thick media. We discuss Doppler broadening first.

A. Doppler broadening

In a Doppler-broadened medium, atoms with different velocities see different one-photon and two-photon detunings. The one-photon detuning becomes

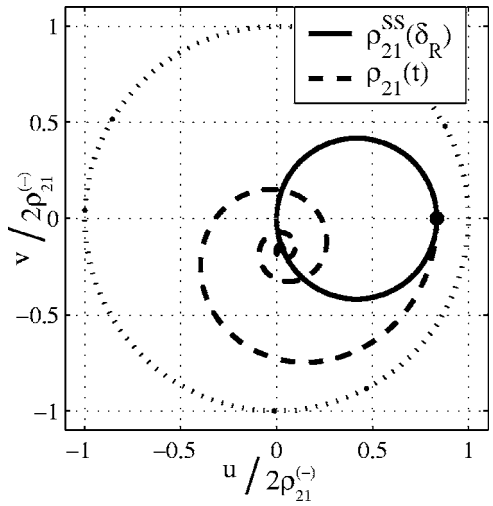

FIG. 4. The spiral pattern of the atomic coherence for the case $\Delta=0$, $\Omega_C=10^{-2}\gamma$, $\Omega_P=10^{-3}\gamma$, $\Gamma=10^{-5}\gamma$, and $\delta_R=-3\Omega^2/\gamma \approx -3/2R$. The dashed line shows the path taken by $\rho_{21}(t)$ as a function of time. The solid circle shows all possible steady-state values for ρ_{21} with each point along the circle corresponding to a different value of δ_R and all other parameters remaining fixed. Finally, the dotted circle shows the maximum possible values for $\rho_{21}(t)$.

$$\Delta(v) = \Delta(0) + \frac{v}{2c}(2\omega_3 - \omega_1 - \omega_2),$$

and the two-photon detuning becomes

$$\delta_R(v) = \delta_R(0) + \frac{v}{c}(\omega_1 - \omega_2)/c + \frac{\Omega_S^2}{\Delta_S + \frac{v}{c}(\omega_3 - \omega_2)},$$

where v is the velocity of the atom (not to be confused with second element in the Bloch vector). Thus, different velocity classes will oscillate and relax to steady state at different rates due to the dependence of R and T on these detunings. The total susceptibility is found by integrating over all velocities classes,

$$\chi_P = \frac{1}{\sqrt{2\pi}v_p}\int_{-\infty}^{\infty} dv\ \chi_p(v)\exp(-v^2/2v_p^2), \tag{38}$$

where v_p is the most probable velocity.

One significant effect of Doppler broadening is seen in the large-torque regime, where oscillations of the susceptibilities damp out faster than for a single velocity. The velocity dependence of $T(v)$ creates phase diffusion among the ground-state coherences for atoms of different velocity classes. This phase diffusion is similar to free-induction decay. Another factor contributing to the rapid oscillation decay is that each velocity class begins its evolution with a different phase $\phi(v)$. Like spin echoes in free-induction decay, a dark-state echo can be created in an EIT medium at time $t=t_f$ by changing the sign of the Stark shift at time $t=t_f/2$.

Other effects of Doppler broadening result from Doppler narrowing of the EIT line. Since Doppler narrowing of EIT lines has been discussed at length elsewhere [37], we do not discuss it here.

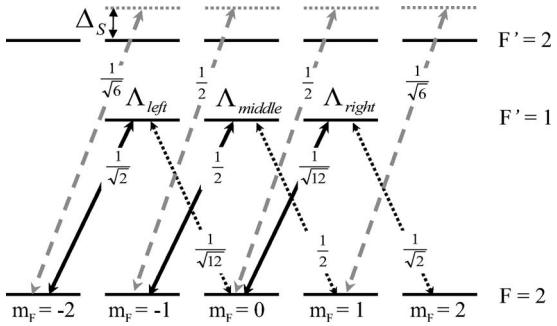

FIG. 5. The dipole moment elements for the EIT cross-phase modulation using the $D1$ line in ^{87}Rb. See text for a description of the transitions.

B. Multilevel systems

The same principles which describe EIT Kerr transients in Λ systems also apply in more complex systems. As the complexity of the system increases, an intuitive physical picture becomes more important because solving the complete density matrix, although possible, becomes algebraically less tractable and less insightful. Thus, it is helpful to be able to make some intuitive physical arguments about the fields and atoms without solving the exact density matrix.

As an example of a realistic atomic system we consider the $D1$ line in ^{87}Rb shown in Fig. 5. EIT is created by the coupling (solid black lines) and probe (dotted black lines) fields which have the same frequency but opposite polarizations. The coupling (probe) field is σ^+ (σ^-) polarized and is resonant with the $|F=2\rangle \leftrightarrow |F'=1\rangle$ transitions. The signal field (dashed gray lines) is detuned from the $|F=2\rangle \leftrightarrow |F'=2\rangle$ transition and is also σ^+ polarized. For simplicity we assume the probe and coupling fields have equal intensities.

As seen in Fig. 6, the transients of the probe susceptibility are more complicated than a damped simple harmonic oscillator. The complexity of the transients is most evident in the spiral plot (see Fig. 6, inset), in which the real and imaginary parts of the susceptibility are plotted parametrically as a function of time. The rich structure of these transients arises from multiple two-photon detunings.

These transients can be understood as a simple extension of the Λ system by subdividing the EIT system into three Λ systems corresponding with transitions directly involving the three EIT excited states ($|^{F'=1}_{m=-1}\rangle$, $|^{F'=1}_{m=0}\rangle$, and $|^{F'=1}_{m=1}\rangle$). In Fig. 5 the excited state of each Λ is explicitly labeled. Two of the Λ's are the left and right halves of the M dark state,

$$|M\rangle = \frac{\left|\begin{matrix}F=2\\m=-2\end{matrix}\right\rangle - \sqrt{6}\left|\begin{matrix}F=2\\m=0\end{matrix}\right\rangle + \left|\begin{matrix}F=2\\m=2\end{matrix}\right\rangle}{\sqrt{8}}, \tag{39}$$

and the third Λ is the middle or Λ dark state:

$$|\Lambda\rangle = \frac{\left|\begin{matrix}F=2\\m=-1\end{matrix}\right\rangle - \left|\begin{matrix}F=2\\m=1\end{matrix}\right\rangle}{\sqrt{2}}. \tag{40}$$

Although the state $|M\rangle$ is in reality a single dark state, for understanding EIT Kerr transients it is more helpful to think

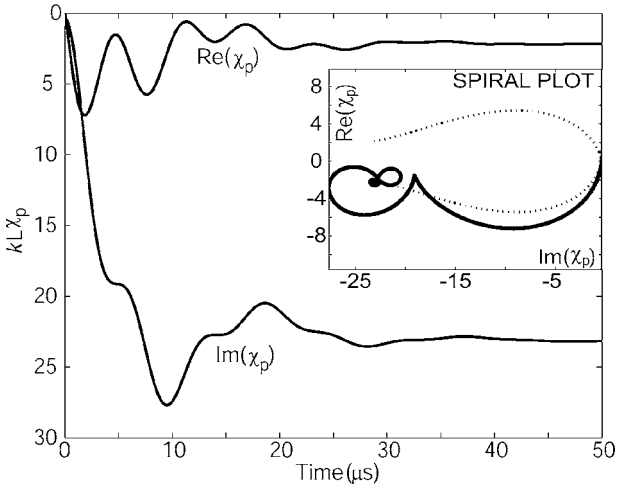

FIG. 6. Evolution of the real and imaginary parts of the probe susceptibility for EIT on the $D1$ line in ^{87}Rb. Before time $t=0$ the system is in steady state with $\Omega_P=\Omega_C=\gamma/10$ and $\Gamma=\gamma/100$. For time $t>0$ a signal field $\Omega_S=\gamma/10$ detuned by $\Delta_S=100\gamma$ Stark-shifts the ground states. The inset shows a parametric plot of real part of the susceptibility versus the imaginary part plotted parametrically as a function of time for $0\leqslant t\leqslant 50$ μs. $L=1$ cm and $N=10^{16}$ m^{-3}.

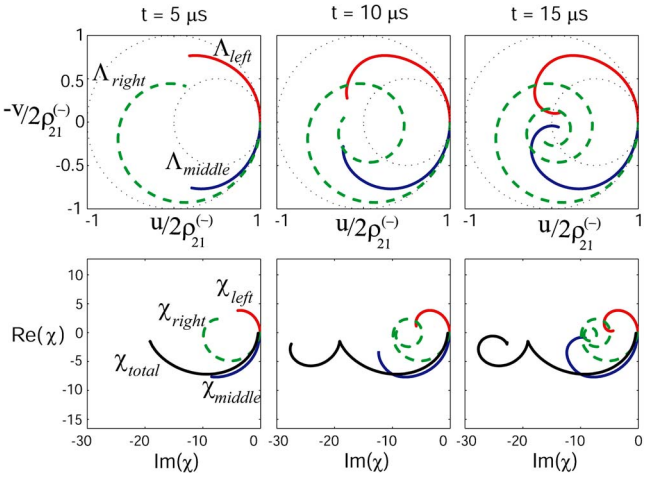

FIG. 7. (Color online) Parametric (spiral) plots of the probe susceptibility (bottom) and ground-state coherences (top) plotted real part versus imaginary part as a function of time. Plots are shown for times $t=5$ μs, $t=10$ μs, and $t=15$ μs. The ground-state coherences (top) are normalized by their initial magnitude. The total probe susceptibility (bottom) (χ_{total}) is the sum of individual susceptibilities for the $|^{F=2}_{m=0}\rangle\leftrightarrow|^{F'=1}_{m=-1}\rangle$ (χ_{left}), $|^{F=2}_{m=1}\rangle\leftrightarrow|^{F'=1}_{m=0}\rangle$ (χ_{middle}), and $|^{F=2}_{m=2}\rangle\leftrightarrow|^{F'=1}_{m=1}\rangle$ (χ_{right}) transitions. The susceptibilities are not normalized and are plotted with arbitrary units.

of $|M\rangle$ as two dark states corresponding to Λ_{left} and Λ_{right}.

Each sublevel of the ground state experiences a different Stark shift determined by the dipole moments for the signal transitions. Thus, each Λ experiences a different two-photon detuning: $\delta_{middle}=\Omega_S^2/12\Delta_S$, $\delta_{left}=-\Omega_S^2/12\Delta_S$, and $\delta_{right}=\Omega_S^2/4\Delta_S$. Figure 7 shows a progression for the spiral plots of the ground-state coherences (top) and probe susceptibilities (bottom) at times 5 μs, 10 μs, and 15 μs. The ground-state coherences are normalized by their initial value. Both Figs. 6 and 7 were obtained by solving the complete density matrix numerically. However, Fig. 7 is almost exactly what we find if we apply the three-level theory to each Λ separately. The coherence for each individual Λ—i.e., Λ_{left}, Λ_{middle}, and Λ_{right}—spirals as predicted by Eqs. (23) and (24) and each individual susceptibility—i.e., χ_{left}, χ_{middle}, and χ_{right}—follows its corresponding coherence as predicted by the three-level theory in Eqs. (30) and (31).

Although the dynamics of each individual Λ is simple, the superposition of different Λ's with their Stark shifts of differing signs and magnitudes creates a total susceptibility with complex dynamics. Because the left and middle coherences rotate in opposite directions with the same frequency, the coherence terms v_{left} and v_{middle} destructively interfere while u_{left} and u_{middle} constructively interfere, which is why $\mathrm{Re}(\chi_p)$ is much smaller than $\mathrm{Im}(\chi_p)$ in Fig. 6. Also, the fact that Λ_{right} rotates 3 times as fast as the other Λ's is the source of the nonsinusoidal periodic oscillations.

Initially, the population is shared between the $|M\rangle$ and $|\Lambda\rangle$ dark states in an approximately 50%-50% ratio. The population of state $|M\rangle$ is spread approximately equally between Λ_{left} and Λ_{right}, which is the reason the Λ_{middle} susceptibility is roughly twice as large either Λ_{left} or Λ_{right}. In the bottom plot it is straightforward to see that the total susceptibility χ_{total} is simply the sum of susceptibilities for each Λ. Thus, by treating each Λ separately we could have estimated the dynamics of the entire system rather than solving the density matrix exactly.

C. Optically thick media

One advantage of the refractive EIT Kerr nonlinearity is that an arbitrarily long medium of constant optical density should provide an arbitrarily large cross-phase shift of the probe field, even for an arbitrarily small signal field. For this reason few-photon applications of EIT Kerr effects generally assume optically thick media. In this section we restrict our analysis to small Stark shifts—i.e., the small-torque regime. Also, we only consider signal pulse durations such that the pulse is much longer than the medium.

For optically thick media we must consider the dynamics of the fields in addition to atomic evolution. The interaction between medium and fields lengthens the rise time proportionally to the optical thickness. The increased rise time can be seen in numerical simulations of the coupled Maxwell-density-matrix equations, but it can also be accurately estimated using the three-level theory presented in this paper.

The rise times may be found by first solving for the steady-state phase of the ground-state coherences and then taking the ratio between the phase rotation angle and the phase rotation rate ($t_u\approx t_v\approx\Delta\theta/\dot{\theta}$). This is similar to the discussion of rise times for optically thin media.

For resonant cw fields, the susceptibilities are

$$\chi_P\approx -i\frac{\sigma_{32}c}{\omega_{32}}\rho_{22}(1-\rho_{21}/\rho_{21}^{(-)})^* \tag{41}$$

and

$$\chi_C \approx -i\frac{\sigma_{31}c}{\omega_{31}}\rho_{11}(1-\rho_{21}/\rho_{21}^{(-)}), \tag{42}$$

where the cross sections are $\sigma_{32}=N|\mu_{32}|^2\omega_{32}/\epsilon_0 c\hbar\gamma$ and $\sigma_{31}=N|\mu_{31}|^2\omega_{31}/\epsilon_0 c\hbar\gamma$. In the slowly-varying-envelope approximation, the Maxwell equations for the evolution of the fields are

$$\left(\frac{\partial}{\partial z}+\frac{1}{c}\frac{\partial}{\partial t}\right)\Omega_P=-\frac{\sigma_{32}\rho_{22}}{2}\left(1-\frac{\rho_{21}^*}{\rho_{21}^{(-)*}}\right)\Omega_P \tag{43}$$

and

$$\left(\frac{\partial}{\partial z}+\frac{1}{c}\frac{\partial}{\partial t}\right)\Omega_C=-\frac{\sigma_{31}\rho_{11}}{2}\left(1-\frac{\rho_{21}}{\rho_{21}^{(-)}}\right)\Omega_C. \tag{44}$$

Assuming negligible absorption (this assumption is implied by the previous assumptions of small torque $T\ll 1$ and the EIT condition $\Omega^2\gg\gamma\Gamma$), we can make the approximation $|\Omega_P(z)|\approx|\Omega_P(0)|$, and Eq. (43) can be integrated to obtain

$$\begin{aligned}\Omega_P(z)&\approx\Omega_P(0)e^{-\sigma_{32}\rho_{22}^{(-)}\left[z-\int_0^z\rho_{21}^*(z')/\rho_{21}^{(-)*}(z')dz'\right]}\\&\approx\Omega_P(0)e^{-z\sigma_{32}\rho_{22}^{(-)}\{i\Delta\theta\}},\end{aligned} \tag{45}$$

where we have used the fact that in steady state the ratio $\rho_{21}(z)/\rho_{21}^{(-)}(z)\approx e^{i\Delta\theta}$ for all z and $\Delta\theta=\delta_R/(R+\Gamma)$ is the thin-medium phase rotation angle for the ground-state coherence. Similarly,

$$\Omega_C(z)\approx\Omega_C(0)e^{-z\sigma_{31}\rho_{11}^{(-)}(-i\Delta\theta)}. \tag{46}$$

Finally, the ground-state coherence as a function of position is

$$\begin{aligned}\rho_{21}(z)&=e^{i\Delta\theta}\rho_{21}^{(-)}(z)\\&=-e^{i\Delta\theta}\frac{\Omega_C(z)\Omega_P^*(z)}{\Omega^2}\\&\approx\rho_{21}^{(-)}(0)e^{i\Delta\theta[1+z(\sigma_{31}\rho_{11}^{(-)}+\sigma_{32}\rho_{22}^{(-)})]}.\end{aligned} \tag{47}$$

Letting $\sigma=\sigma_{31}=\sigma_{32}$, Eq. (47) simplifies to

$$\rho_{21}(z)\approx\rho_{21}^{(-)}(0)\exp[i\Delta\theta(1+\sigma z)]. \tag{48}$$

There are two rise times that must be considered: the rise time of the ground-state coherence phase and the rise time of the field phases (the field phase shift is the refractive Kerr effect). The rise time for the coherences monotonically increases with position z. This is because for larger z, the coherence must rotate through a larger rotation angle $\Delta\theta(z)=\delta_R(1+\sigma z)/(R+\Gamma)$, but the rotation rate $\dot{\theta}\approx\delta_R$ is independent of position. Thus, for optically thick media the coherence $1/e$ rise time is

$$t_u(z)\approx t_v(z)\approx(1-e^{-1})(1+\sigma z)/(R+\Gamma). \tag{49}$$

The rise time for the refractive Kerr effect—i.e., the rise time for the phase of the field leaving the medium—is almost equal to the rise time for the ground-state coherences at $z=L$, where L is the length of the medium. Figure 8 shows the phase of the ground-state coherence and probe field as a function of position along an optically thick medium at several different times. At $z=L$ for early times in the evolution, the phase of the probe field and the phase of the medium ground-state coherence are equal. This is because the size of the Kerr effect is given by the area between the coherence and field phase curves in Fig. 8. For early times in the evolution, the Kerr effect due to the medium near $z=0$ maintains the EIT phase condition [i.e., $\rho_{21}^{(-)}(z)/\rho_{21}(z)=1$] for the downstream medium and the downstream medium does not contribute to the Kerr effect (i.e., it contributes zero "area"). As the system evolves the length of medium contributing to the Kerr effect grows until steady state is reached (in Fig. 8 steady state corresponds to times $t\geqslant 64$ μs) and there is a uniform phase difference between the ground-state coherence and fields along the entire medium. Based on these considerations, the $1/e$ rise time for the Kerr effect in an optically thick medium is approximately given by

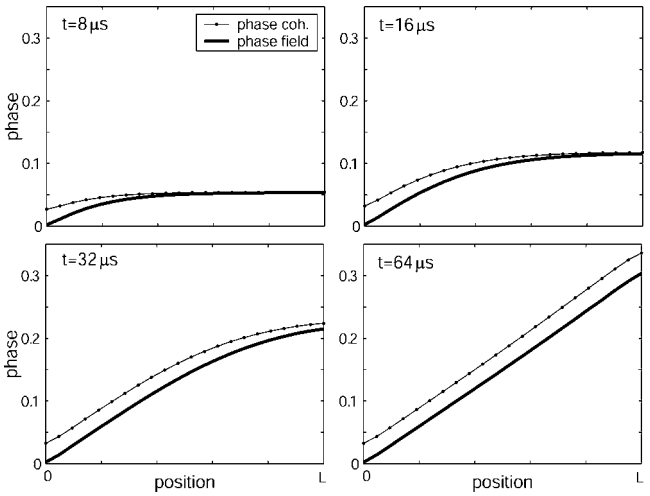

FIG. 8. Snap shots at times $t=8$ μs, $t=16$ μs, $t=32$ μs, and $t=64$ μs of the field phase (thick solid line) and ground-state coherence phase (thin solid line with dots) for an optically thick medium. The EIT fields are traveling from left to right. The evolution of the fields and atoms was simulated numerically using the finite-element method (FEM) Crank-Nicholson algorithm with staggered time steps for the fields and medium.

$$t_{Kerr}\approx(1-e^{-1})\frac{\sigma L}{(R+\Gamma)}. \tag{50}$$

The linear relationship between the EIT Kerr rise time and the optical thickness sets some limitations on potential applications. For example, given a particular signal pulse duration the largest Kerr phase shift achievable is limited to the optical depth for which the rise time and pulse durations are equal. In cw one can theoretically make the Kerr phase shift arbitrarily large by making the medium arbitrarily optically thick.

However, this limitation on the EIT Kerr effect for pulsed beams may not be absolute. It may be possible to use some slow-light tricks with EIT and signal pulses in order to increase the interaction time of the signal in the medium as suggested by Lukin and Imamoglu [8]. Also, we have not considered what happens if the medium is sufficiently long

that the signal pulse can be entirely contained within the medium, which may lead to different results.

V. SUMMARY

In summary, we have discussed refractive EIT Kerr transients for the case of a square signal pulse ac Stark shifting a Λ-EIT system with cw EIT fields. When all fields are well below saturation the four-level EIT Kerr system can be reduced to a two-level Bloch-vector equation and solved analytically. By parametrically plotting the real and imaginary parts of the optical susceptibilities, it is seen that the trajectory of the EIT Kerr transients is a spiral from their initial state to their final-steady-state value. As a function of time, the real and imaginary parts of the susceptibilities are damped sinusoids and the refractive EIT Kerr rise time is approximately given by the inverse of the optical pumping rate R (this rise time is valid as along as the optical pumping rate is much larger than the two-photon or Raman detuning—i.e., $R \gg \delta_R$).

Although the intuitive picture of "spiraling" optical susceptibilities was derived for a four-level system, it can also be applied to more experimentally realistic and complex models. In particular, we have considered how Doppler broadening, additional levels, and optically thick media modify the refractive EIT Kerr transients. Doppler broadening damps out the coherence oscillations more quickly than for atoms of a single-velocity class. The EIT Kerr system with additional levels can result in coherence oscillations with rich structure due to differing two-photon detunings. Finally, optically thick media have much longer rise times than optically thin media because the ground-state coherences for the atoms at the end of the medium must pass through a much larger phase rotation. In the limit that $R \gg \delta_R$, the refractive EIT Kerr rise time in optically thick media is proportional to the optical thickness and inversely proportional to the optical pumping rate.

ACKNOWLEDGMENTS

This work was supported by DARPA Slow Light, the National Science Foundation, and Research Corporation.

[1] P. R. Hemmer, D. P. Katz, J. Donoghue, M. Cronin-Golomb, M. S. Shahriar, and P. Kumar, Opt. Lett. **20**, 982 (1995).
[2] Y.-Q. Li and M. Xiao, Opt. Lett. **21**, 1064 (1996).
[3] M. Jain, H. Xia, G. Y. Yin, A. J. Merriam, and S. E. Harris, Phys. Rev. Lett. **77**, 4326 (1996).
[4] S. E. Harris and L. V. Hau, Phys. Rev. Lett. **82**, 4611 (1999).
[5] M. D. Lukin and A. Imamoglu, Nature (London) **413**, 273 (2001).
[6] M. Fleischhauer, A. Imamoglu, and J. P. Marangos, Rev. Mod. Phys. **77**, 633 (2005).
[7] H. Schmidt and A. Imamoglu, Opt. Lett. **21**, 1936 (1996).
[8] M. D. Lukin and A. Imamoglu, Phys. Rev. Lett. **84**, 1419 (2000).
[9] D. Petrosyan and G. Kurizki, Phys. Rev. A **65**, 033833 (2002).
[10] A. B. Matsko, I. Novikova, G. R. Welch, and M. S. Zubairy, Opt. Lett. **28**, 96 (2003).
[11] R. G. Beausoleil, W. J. Munro, and T. P. Spiller, J. Mod. Opt. **51**, 1559 (2004).
[12] S. E. Harris and Y. Yamamoto, Phys. Rev. Lett. **81**, 3611 (1998).
[13] J.-Q. Shen, Z.-C. Ruan, and S. He, Phys. Lett. A **330**, 487 (2004).
[14] M. Yan, E. G. Rickey, and Y. Zhu, Phys. Rev. A **64**, 041801(R) (2001).
[15] D. A. Braje, V. Balic, G. Y. Yin, and S. E. Harris, Phys. Rev. A **68**, 041801(R) (2003).
[16] Y.-F. Chen, G.-C. Pan, and I. A. Yu, Phys. Rev. A **69**, 063801 (2004).
[17] H. Schmidt and A. Imamoglu, Opt. Lett. **23**, 107 (1998).
[18] L. Deng, M. G. Payne, and W. R. Garrett, Phys. Rev. A **64**, 023807 (2001).
[19] C. Ottaviani, S. Rebic, D. Vitali, and P. Tombesi, Phys. Rev. A **73**, 010301(R) (2006).
[20] Y.-F. Chen, G.-C. Pan, and I. A. Yu, J. Opt. Soc. Am. B **21**, 1647 (2004).
[21] S. J. Park, H. Cho, T. Y. Kwon, and H. S. Lee, Phys. Rev. A **69**, 023806 (2004).
[22] A. Godone, S. Micalizio, and F. Levi, Phys. Rev. A **66**, 063807 (2002).
[23] K. Harada, K. Motomura, T. Koshimizu, H. Ueno, and M. Mitsunaga, J. Opt. Soc. Am. B **22**, 1105 (2005).
[24] M. O. Scully, S.-Y. Zhu, and A. Gavrielides, Phys. Rev. Lett. **62**, 2813 (1989).
[25] M. Kash, V. A. Sautenkov, A. S. Zibrov, L. Hollberg, G. R. Welch, M. D. Lukin, Y. Rostovtsev, E. S. Fry, and M. O. Scully, Phys. Rev. Lett. **70**, 3235 (1993).
[26] Y. Zhu, Phys. Rev. A **53**, 2742 (1995).
[27] P. Valente, H. Failache, and A. Lezama, Phys. Rev. A **65**, 023814 (2001).
[28] A. S. Zibrov and A. B. Matsko, Phys. Rev. A **64**, 013814 (2001).
[29] A. Mair, J. Hagen, D. F. Phillips, R. L. Walsworth, and M. D. Lukin, Phys. Rev. A **65**, 031802(R) (2002).
[30] K. Bergman, H. Theuer, and B. W. Shore, Rev. Mod. Phys. **70**, 1003 (1998).
[31] N. V. Vitanov, T. Halfmann, B. W. Shore, and K. Bergman, Annu. Rev. Phys. Chem. **52**, 763 (2001).
[32] M. Lindberg and R. Binder, Phys. Rev. Lett. **75**, 1403 (1995).
[33] Y. Wu and X. Yang, Phys. Rev. A **71**, 053806 (2005).
[34] E. A. Korsunsky, N. Leinfellner, A. Huss, S. Baluschev, and L. Windholz, Phys. Rev. A **59**, 2302 (1999).
[35] W. Maichen, F. Renzoni, I. Mazets, E. Korsunsky, and L. Windholz, Phys. Rev. A **53**, 3444 (1996).
[36] R. S. Bennink, Ph.D. thesis, Institute of Optics, University of Rochester, 2004.
[37] A. Javan, O. Kocharovshaya, H. Lee, and M. O. Scully, Phys. Rev. A **66**, 013805 (2002).